The wettability and phosphate adsorption characteristics of katoite in RM were studied by first-principle calculations

Xiaotian Zhou
Guizhou University
Longjiang Li (mnlljiang@163.com)
Guizhou University https://orcid.org/0000-0002-9222-986X
Yueqin Qiu
Guizhou University
Wanshuang Liu
Guizhou University

Research Article

Keywords: red mud, katoite, density functional theory, molecular dynamics, wettability, adsorption

Posted Date: April 11th, 2022

DOI: https://doi.org/10.21203/rs.3.rs-1526489/v1

The wettability and phosphate adsorption characteristics of katoite in RM were studied by first-principle calculations

Zhou Xiaotian [1, 2, 3] Li Longjiang [1, 2, 3*] Qiu Yueqin [1, 2, 3] Liu Wanshuang[1, 2, 3]

[1.]School of Mining, Guizhou University, Guiyang 550025, Ghina

[2.]Guizhou Key Laboratory of Comprehensive Utilization of Non-metallic Mineral Resources, Guiyang 550025, China

3.National & Local Joint Engineering Laboratory for Efficient Utilization of Superior Mineral Resources in Karst Regions, Guizhou, Guiyang 550025, China

*mnlljiang@163.com

Abstract: Red mud (RM) alone as an adsorbent for phosphorus shows unsatisfactory adsorption performance. This paper studied the wettability of katoite (the main component of RM) and its adsorption of phosphate. We also analysed the adsorption law of phosphate-containing water clusters on the katoite surface from bond length changes of the unit cell, adsorption equilibrium conformation, radial distribution function, interaction energy, adsorption isotherm and adsorption heat. found that kattenite has good wettability and the adsorption of phosphate is the result of van der Waals force and hydrogen bond.

Keywords: red mud, katoite, density functional theory, molecular dynamics, wettability, adsorption.

1 Introduction

Red mud (RM) is a solid waste product from the industrial production of Al_2O_3, which acquires its name because it is brown or russet due to iron oxide. RM is mainly produced by the Bayer method worldwide[1]. The specific surface area of RM measured by the Brunauer–Emmett–Teller (BET) method is about 10~25 m^2g. Particle size analysis by laser diffraction reveals that particles with a diameter of less than 2 μm account for more than 60% of RM. Because of its small particle size, large specific surface area and multiphase mineral composition, RM has a unique cemented porous structure

with high porosity, demonstrating a certain adsorption capacity. Compared with traditional and commonly used adsorbents, RM is more economical and environmentally friendly.

However, RM alone as an adsorbent for phosphorus shows unsatisfactory adsorption performance. Studies have shown that the unmodified RM surface has a poor wetting effect, low activity and a small specific surface area. Moreover, basic groups on the RM surface result in more negative charges of RM under high-pH conditions, which enhances the repulsion of phosphate and thereby leads to unsatisfactory phosphorus adsorption performance of the undisturbed RM[2, 3]. However, RM can be used as the main material to adsorb phosphorus-containing wastewater. Many scholars have researched this. In 1977, Shiao and Akashi[4] first proposed to use hydrochloric-acid-acidified RM to adsorb excess phosphorus in water. Subsequently, Verma et al[5]. used orthogonal flow microfiltration to remove phosphate in water. Wang[6] and Zhao [7]used RM as the main raw material for acid thermal activation and developed a new type of RM particle adsorption material for removing phosphorus in water bodies. However, the introduction of excessive acidic substances and the use of high temperature in acid thermal activation increase the adsorption cost, and the preparation and adsorption of acid thermal activation increase the environmental risk of the entire adsorption system.

Studies on the adsorption behaviour of RM as the main adsorbent material mostly adopt modern instrumental analysis to illustrate the bonding or physical or chemical adsorption between phosphate and certain RM components[8, 9]. This paper studies the reasons for the unsatisfactory adsorption performance of undisturbed RM from the perspective of wettability. Both wettability and adsorption energy provide strong evidences to explain adsorption. Taking Katoite, the main substance in the undisturbed RM, as the research object, we study the wettability of Katoite and its adsorption against phosphate from a microscopic point of view. Thierfelder、Qiu、Zhang et alperformed molecular simulations to study the adsorption of gas by the pore structure. Thierfelder [10] studied the adsorption of graphite on the methane surface using grand canonical Monte Carlo simulations and predicted the adsorption isotherms of methane at different temperatures and pressures. Qiu[11] used density functional theory (DFT) to study the adsorption behaviour of methane gas on the coal surface model and found that the interaction energy increases as the adsorbate system increases. Zhang[12] calculated the dynamics relaxation of gas molecules on the adsorbate in the range of 0.1–10

Mpa and found that when the pressure is more than 8 Mpa, the adsorption amount of gas molecules remains unchanged.

This paper studied the reasons for the unsatisfactory adsorption performance of undisturbed RM from the perspective of wettability. Both wettability and adsorption energy provide strong evidence to explain adsorption. Taking katoite, the main component of undisturbed RM, as the research object, we studied the wettability of katoite and its adsorption of phosphate from a microscopic point of view.

Due to the complex characteristics of RM components, we used Materials Studio simulation software to study the crystal structure of katoite. Few studies have used molecular dynamics (MD) to simulate the wettability of the katoite surface and its adsorption of phosphate. Through simulation calculations based on DFT and MD, we analysed the adsorption law of water clusters and phosphate-containing water clusters on the katoite surface from bond length changes[13-15] of the unit cell, adsorption equilibrium conformation[16-18], radial distribution function (RDF)[19-21], interaction energy[22, 23], adsorption isotherm[24] and adsorption heat[25, 26]. According to the wettability characteristics, the process and mechanism of action of phosphate on the katoite surface were also analysed[27].

2 Materials and Methods

2.1 Materials

Katoite belongs to the hydrogrossularite group of minerals and has a cubic crystal structure[28]. RM was obtained from Guizhou Huajin Aluminum Co., Ltd. (China). After drying at 50°C for 12 h with a moisture content of 30%, the RM was ground using a planetary ball mill to a thickness of 0.075 mm and then sieved.

2.2 X-ray diffraction analysis

X-ray diffraction (XRD; PANalytical, X'Pert PRO, UK) was performed for qualitative and quantitative analyses of the phase and crystal structure of RM. The raw data were processed using Jade software according to the Powder Diffraction File database, followed by peak fitting and mineral composition identification. A Cu target Kα ray source (λ = 0.154 nm) with a tube voltage of 40 kV and

a tube current of 40 mA was used. Step scanning was adopted with a step size of 0.05, a scan speed of 0.5°/s and a scan range of 10°–70°.

2.3 Scanning electron microscopy–X-ray energy spectrum analysis

Scanning electron microscopy (SEM; ZEISS Merlin Compact, Germany) was performed to examine the surface structure of RM. X-ray energy spectroscopy (EDS; Oxford X-MAX-20 mm^2, UK) was performed to determine the elemental composition distribution on the RM surface. The characteristic X-rays emitted by different elements have different frequencies, that is, different energies, and the elements can be determined only by the energy detection of different photons. The element content was determined by quantitative analysis without standard samples. The point analysis method of an X-ray energy spectrometer supports the simultaneous detection of multiple elements, with a fast analysis speed, a small analysis volume and high sensitivity, so it was used for rapid fixed-point or microarea element analysis of RM to determine the presence of katoite[29, 30].

2.4 Model selection and calculation

The crystal unit cell of katoite was derived from the FindIt database, and models of PO_4^{3-}, HPO_4^{2-} and $H_2PO_4^{1-}$ ions were plotted using Materials Studio simulation software. The constructed models were subjected to geometry optimisation to find the reasonable molecular structure of the system and the configuration under the state of minimum energy so that dynamics calculation could be performed.

The CASTEP module in Materials Studio was used for geometry optimisation of the models based on DFT. Local density approximation (LDA) and generalised gradient approximation (GGA) were selected for functional methods, including LDA-CA-PZ, GGA -RPBE, GGA-PBESOL, GGA-PBE, GGA-PW91 and GGA-WC. To calculate the exchange correlation functional, the fixed cut-off energy was set to 380 eV and the *k*-point in the Brillouin zone was set to 1 × 1 × 1.

In terms of the geometrically optimised configuration, the adsorption behaviour of phosphate-containing water clusters on the surface model of katoite and wetting-modified katoite was subjected to dynamics relaxation with the Forice module. The precision control was set to ultrafine, the canonical ensemble (NVT) was selected, the initial speed was set to random at a time step of 1 fs, the

total calculation time was 50 ps, the temperature control function was Nose (by constant temperature calculation, the real NVT ensemble is achievable) and the ability field was a COMPASS force field.

At the same time, the Sorption module was used to calculate the adsorption isotherms and stable adsorption sites of PO_4^{3-}, $HPO_4^{2-}$and $H_2PO_4^{1-}$ions on the katoite surface.

3 Results and Discussion

3.1 Phase analysis of RM

As shown in table 1, RM qualitative analysis results based on Rietveld method shows that the minerals from left to right were katoite, calcite, hematite, cancrinite, diaspore, anatase, kaolinite, clinochlore and muscovite. The katoite content was 39.1%, and the lattice constants were $a = b = c =$ 10.8855 Å and $\alpha = \beta = \gamma = 109.4721°$ (space group Ia–3d).

Table 1 RM qualitative analysis results based on Rietveld method

Samples	**Mineral phase content (% by weight wt%)**								
	Katoite	Calcite	Hematite	Cancrinite	Diaspore	Anatase	Kaolinite	Cilnochlore	Muscovite
RM samples	39.1	7.4	5.3	26.1	1.3	1.5	3.6	12.9	3.0

3.2 Scanning electron microscopy and X-ray energy spectrum analysis results

Fig. 1(a) is an enlarged view of the RM surface, and Fig. 1(b) is the EDS spectrum inside the box in Fig. 1(a). Fig. 1(a) shows that the RM surface had an irregular shape, a loose structure and large interparticle voids. Fig. 1(b) shows that the scanning point contained three elements (O, Al and Ca), which is consistent with the main elements in the molecular formula of katoite ($Ca_3Al_{3.5}O_{4.5}(OH)_{7.5}$).

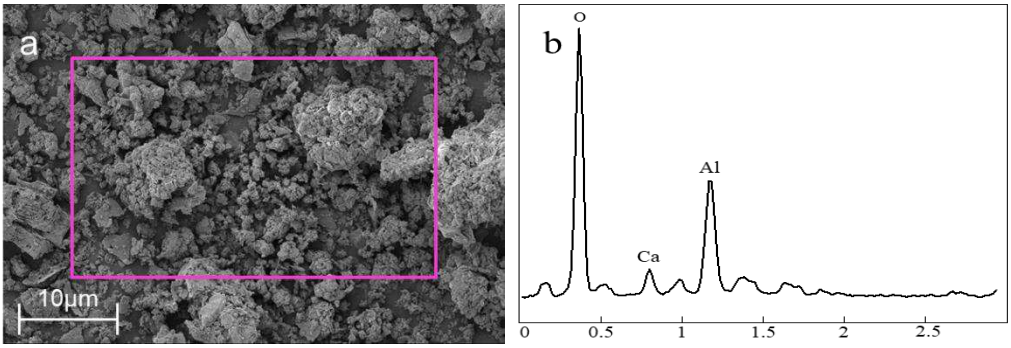

Figure 1 Scanning electron micrograph of RM (a) and X-ray energy spectrum at bright spot (b)

3.3 Geometry optimisation of the adsorption structure

Before dynamics relaxation, the geometry optimisation of different cross-linking functionals was performed on katoite. The total energy of the system is shown in Table 2. The smaller the total energy of the system, the more stable the crystal structure. When katoite adopted the exchange correlation functional GGA-PW91, the system energy was the lowest, that is, the crystal structure was in the most stable state (Table 2). Analysis of the most stable configuration of katoite shows that the valence electron orbital for optimisation of Al and O atoms in katoite is $3s^2 3p^1$. Fig. 2(a) shows the katoite structure before geometry optimisation, in which the Al–O bond length is 1.918 Å. Fig. 2(b) shows the calcium structure after geometry optimisation, in which the A–O bond length is 1.902 Å. The Al–O bonds in the optimised structure were all smaller after optimisation, indicating that the optimised katoite surface possesses stronger electronegativity.

To illustrate in detail the electronic structure on the katoite surface, the density of states (DOS) and the partial density of states (PDOS) were compared. As shown in Fig. 2(b1), the electronic energy levels of katoite were mainly distributed between −40 and 8 eV. According to the distribution characteristics of valence electrons and the number of atoms in the unit cell, the number of theoretical Al atoms of katoite was 8 before optimisation. The number of valence electrons was 26.982 before optimisation and 27 after optimisation. The two were basically the same, indicating balanced distribution of electrons in the overall system. As shown in Fig. 2(b2), a new peak appeared in the partial-wave-state density of O atoms near the Fermi level. Thus, O atoms have higher electronegativity in the katoite system.

Table 2 Total energy of the katoite system under different cross-linking functionals

Name	LDA-CA-PZ	GGA-PBESOL	GGA-RPBE	GGA-PBE	GGA-PW91	GGA-WC
Energy(eV)	−34292.0655	−34330.7725	−34206.1681	−34309.9044	−34336.3608	−34246.8558

LDA, local density approximation; GGA, generalised gradient approximation.

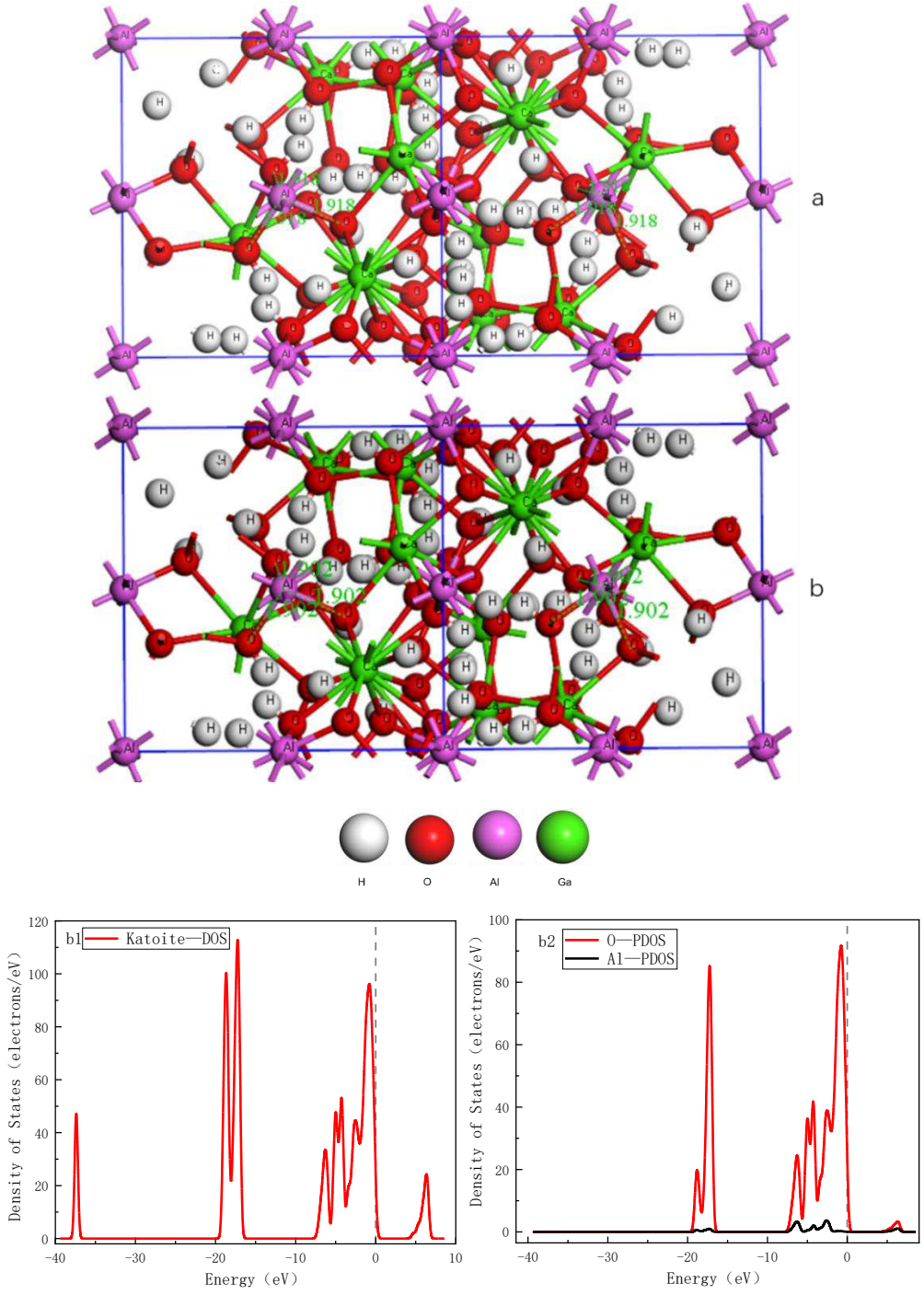

Figure 2 Structure and total density of states (b1) O, Al partial density of states (b2) before (a) and after (b) geometry optimization of Katoite. The dotted line is the Fermi level

3.4 Dynamics relaxation

As the adsorption in the system progresses, the system energy fluctuation gradually stabilises, so it can be used to judge the system balance. Fig. 3 (a) shows the change in system energy with time during dynamics relaxation. The total energy of the three phosphate-containing water clusters stabilised after 5 ps, that is, the system reached equilibrium at 5 ps. In addition, among the three water clusters, the HPO_4^{2-}-containing water cluster possessed the smallest energy when it reached a stable state, followed by the $H_2PO_4^-$-containing water cluster and then the PO_4^{3-}-containing water cluster.

During dynamics relaxation, the three water clusters interacted on the katoite surface and the system configuration changed dynamically. As shown in Fig. 3(b), the three water clusters showed a similar reaction process on the katoite surface. In the initial state, the PO_4^{3-}-, HPO_4^{2-}- and $H_2PO_4^-$-containing water clusters in a1, b1 and c1 were all on the katoite surface. After the reaction, the configuration of water molecules and phosphate in the system changed to downward O atoms. For instance, the PO_4^{3-}-, HPO_4^{2-}- and $H_2PO_4^-$-containing water clusters in a2, b2 and c2, migrated towards the katoite surface and then adsorbed to the crystal surface. Finally, the wetting film on the surface of the phosphate-containing water clusters was broken and the number of hydrogen bonds in the cluster decreased, so the water molecules and phosphate adsorbed to the katoite surface. As shown in Fig. 3,comparison of the PO_4^{3-}-, HPO_4^{2-}- and $H_2PO_4^-$-containing water clusters in a2, d2 and b2 showed that the phosphate-containing water clusters completely spread on and adsorbed to the surface of the wetting-modified katoite, indicating that the katoite surface has significant wettability.

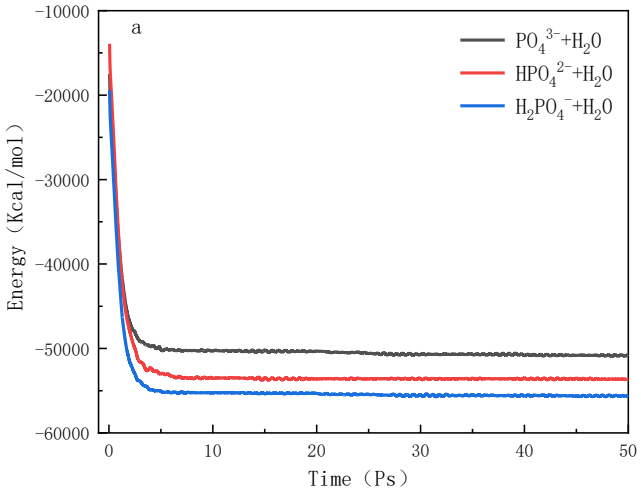

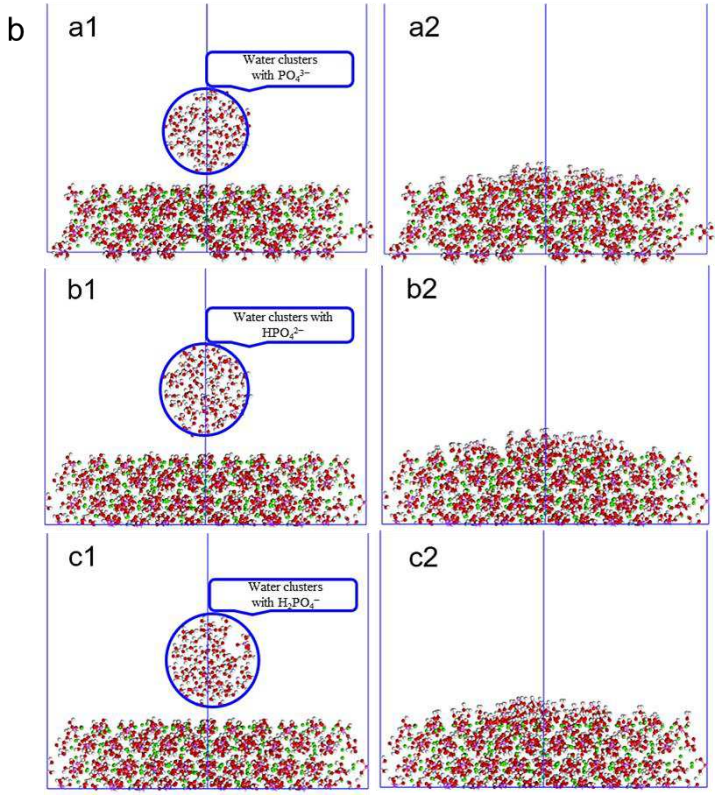

Figure 3 (a)Total energy change of phosphate-containing water clusters on the katoite surface; (b)Dynamics relaxation of phosphate-containing water clusters on the katoite surface. (a1, a2) are PO43−-containing water clusters, (b1, b2) are HPO42−-containing water clusters and (c1, c2) are H2PO4−-containing water clusters.

3.5 Radial distribution function

We thoroughly studied the adsorption distribution characteristics of the three phosphate-containing water clusters on the katoite surface. Fig. 4 reveals the RDFs of O atoms and H_2O on the katoite surface in different phosphate-containing water clusters adsorbed by katoite, as well as O atoms and PO_4^{3-}, $HPO_4^{2-}$and $H_2PO_4^-$. Fig. 4 shows that among the three systems in which katoite and wetting-modified katoite adsorb phosphate-containing water clusters, two obvious peaks appeared in O-H_2O, O-PO_4^{3-}, O-$HPO_4^{2-}$and O-$H_2PO_4^-$. This also confirmed that in geometry optimisation, O atoms on the katoite surface possess higher electronegativity. The peak strength of the RDF of O atoms and phosphate from high to low was as follows: O-PO_4^{3-}, O-$HPO_4^{2-}$and O-$H_2PO_4^-$. This showed that the adsorption capacity of phosphate on the katoite surface from strong to weak is $H_2PO_4^-$> HPO_4^{2-}> PO_4^{3-}

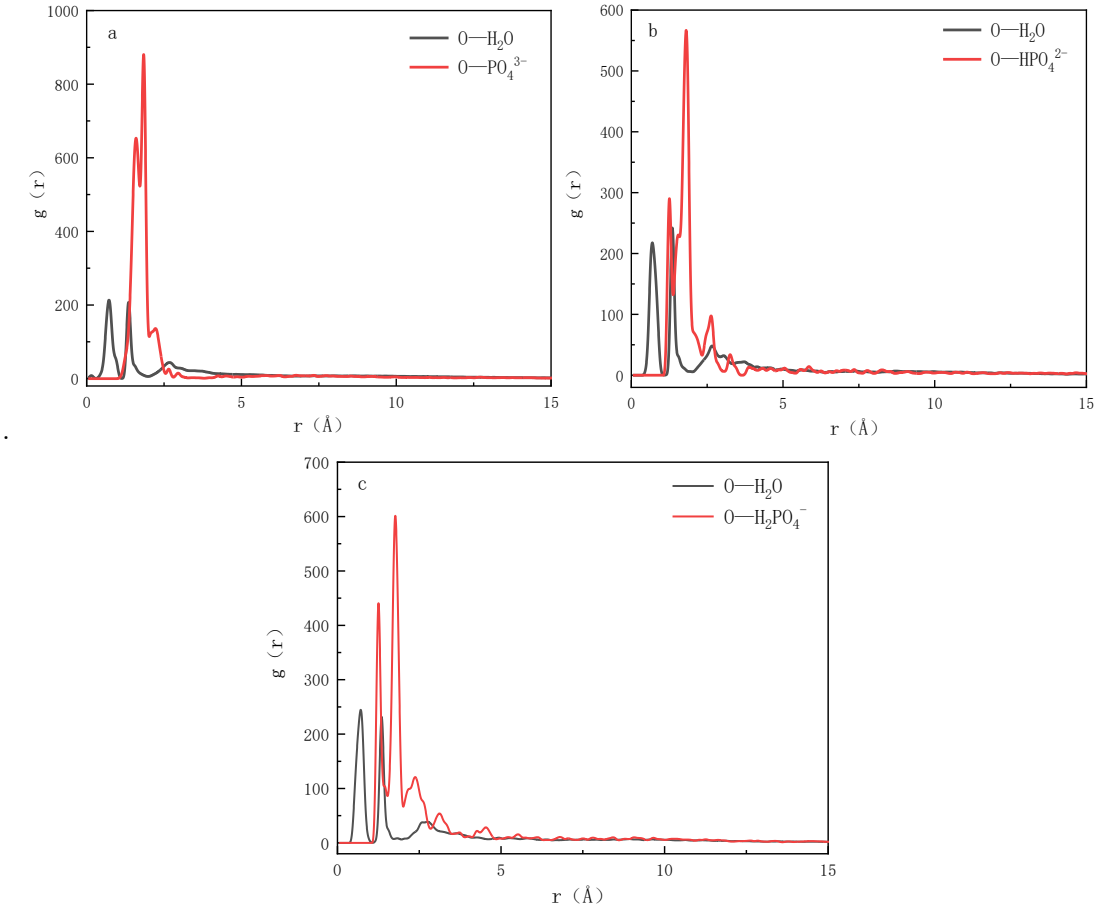

Figure 4 Radial distribution function of phosphate ion (a) hydrogen phosphate ion (b) dihydrogen phosphate ion (c)

3.6 Adsorption energy and adsorption heat

Adsorption energy and adsorption heat are the energy and thermal effects created during the adsorption process. Adsorption is a process in which the molecule moves from fast to slow speed and finally stays on the adsorption medium surface. When the speed decreases, a part of energy and heat is released. This part of energy is known as adsorption energy and adsorption heat, respectively. When interacting with the same mineral surface, different kinds of substances exhibit different surface adsorption energies and adsorption heat. The adsorption strength of phosphate-containing water clusters and the katoite surface can be determined through the adsorption energy and adsorption heat.The adsorption heat in physical adsorption is equal to the sum of the condensation heat and wetting heat of the adsorbate, which is generally several hundred to several thousand joules per mole and does not exceed 40 kJ/mol to the maximum. Adsorption heat is greater in chemical adsorption,

generally 84~417 kJ/mol, than in physical adsorption.

Table 3 shows that katoite had lower adsorption energy for $H_2PO_4^-$-containing water clusters than that for HPO_4^{2-}- and phosphate PO_4^{3-}-containing water clusters, indicating that the katoite surface's adsorption strength of phosphate-containing water clusters is ranked in descending order as $H_2PO_4^-$> HPO_4^{2-}> PO_4^{3-}. Table 3 also shows that the adsorption of $H_2PO_4^-$-and HPO_4^{2-}-to the katoite surface was accompanied by chemical adsorption, while that to PO_4^3-was only physical adsorption.

Table 3 Adsorption energy of the three phosphate-containing water clusters and adsorption heat of the katoite surface

Name	Adsorption energy (Kcal/mol)	Adsorption heat (Kcal/mol)
PO_4^{3-}+H_2O	−50290.1033	41.3099
HPO_4^{2-}+H_2O	−52453.1219	85.8687
$H_2PO_4^-$+H_2O	−53668.1989	88.3281

3.7 Adsorption isotherm

As shown in Fig. 5, the adsorption isotherms of the three phosphate ions on the katoite surface were calculated at 298 K. The adsorption isotherms of PO_4^{3-}, $HPO_4^{2-}$and H_2PO_4 on the katoite surface exhibited type I Langmuir adsorption behaviour. At the same temperature, the adsorption capacity increased with an increase in adsorption pressure. The adsorption capacity of the three phosphate at the same adsorption pressure was ranked in descending order $H_2PO_4^-$> HPO_4^{2-}> PO_4^{3-}.

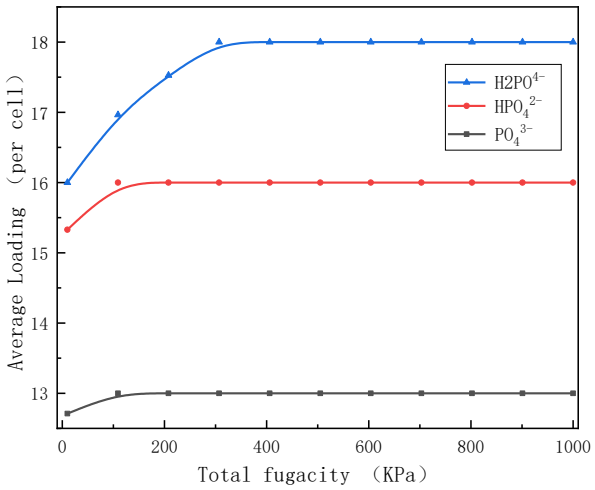

Figure 5 The adsorption isotherms of the three phosphate ions on the Katoite surface

3.8 Adsorption structure

Fig. 6(a–c) shows the structure of PO_4^{3-}, $HPO_4^{2-}$and $H_2PO_4^-$, respectively, adsorbed on the katoite surface. The distance between the oxygen atom in PO_4^{3-}, $HPO_4^{2-}$and $H_2PO_4^-$and the oxygen atom on the katoite surface was ranked in descending order as O_{121}-H = 1.674 Å in $H_2PO_4^-$, O_{120}-H = 1.835 Å in $HPO_4^{2-}$and O_{124}-H = 1.912 Å in PO_4^{3-}. This indicates the presence of hydrogen bond interaction between O atoms of the phosphate and H atoms on the katoite surface. In addition, the adsorption strength of katoite for phosphate was ranked in descending order as $H_2PO_4^-$> HPO_4^{2-}> PO_4^{3-}.

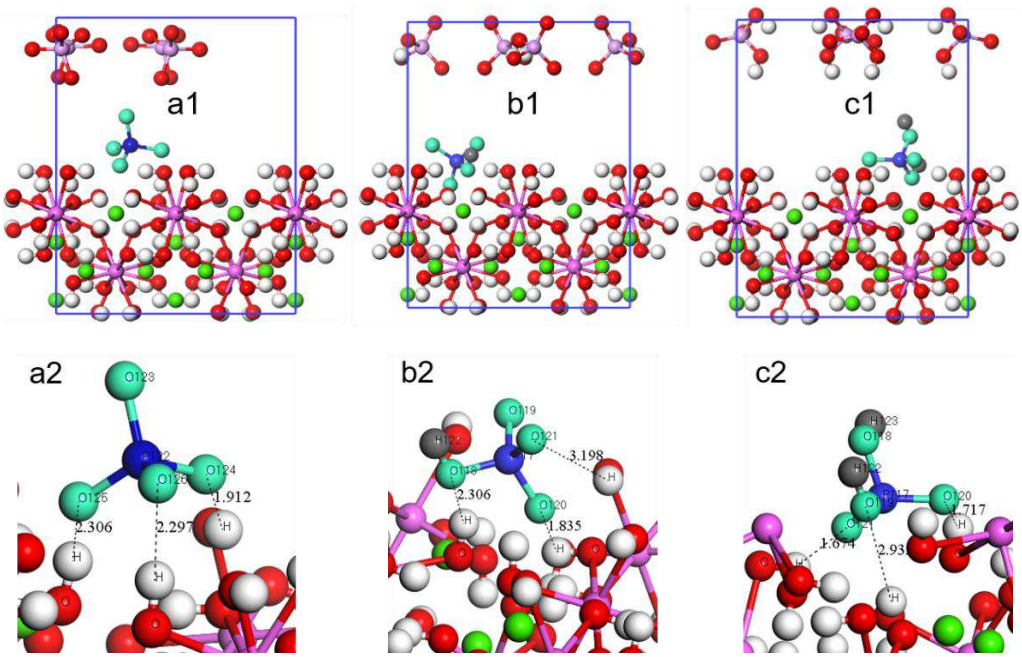

Figure 6 Adsorption configuration of adsorbate on the Katoite surface

4 Conclusion

Using simulation calculations based on DFT and MD, we examined the wetting adsorption characteristics of three water clusters (PO_4^{3-}, $HPO_4^{2-}$and $H_2PO_4^-$) on the katoite surface. The main conclusions are as follows:

(1) The katoite surface has good wettability. The adsorption capacity of katoite for phosphate in descending order is $H_2PO_4^-$> HPO_4^{2-}> PO_4^{3-}.

(2) The adsorption of the katoite surface for $H_2PO_4^-$ and HPO_4^{2-} is accompanied by chemical adsorption, while that for PO_4^{3-} is only physical adsorption. The adsorption conforms to the Langmuir isotherm adsorption model.

(3) The internal cause (mechanism) of the adsorption of phosphate to the katoite surface is the result of the combined effect of van der Waals forces and hydrogen bonds between adsorbent and adsorbate molecules.

Figure Legends

Fig.1 Scanning electron micrograph of RM (RM) (a) and X-ray energy spectrum at the bright spot (b)

Fig. 2 Structure and total density of states (DOS) (b1) and O and Al partial density of states (PDOS) (b2)before (a) and after (b) geometry optimisation of katoite. The dotted line is the Fermi level.

Fig. 3 (a)Total energy change of phosphate-containing water clusters on the katoite surface; (b)Dynamics relaxation of phosphate-containing water clusters on the katoite surface. (a1, a2) are PO_4^{3-}-containing water clusters, (b1, b2) are HPO_4^{2-}-containing water clusters and (c1, c2) are $H_2PO_4^-$-containing water clusters.

Fig. 4 Radial distribution function of PO_4^{3-}(a), HPO_4^{2-}(b) and $H_2PO_4^-$(c)

Fig. 5 Adsorption isotherms of the three phosphate ions on the katoite surface

Fig.6 Adsorption configuration of the adsorbate on the katoite surface

Declarations

Funding: National Natural Science Foundation of China (Program No. 51964010).

Conflicts of interest/Competing interests: On behalf of all authors, the corresponding author states that there is no conflict of interest.

Availability of data and material: The data that support the findings of this study are available upon reasonable request from the authors.

Code availability: Materials Studio.

Authors' contributions: **Zhou Xiaotian:** Conceptualization, Methodology, Formal analysis, Investigation, Data Curation, Writing - Original Draft, Visualization. **Li Longjiang:** Conceptualization, Methodology, Validation, Writing - Review & Editing, Funding acquisition. **Qiu Yueqin:** Conceptualization, Supervision. **Liu Wanshuang:** Formal analysis, Investigation, Data Curation, Visualization.

References

1. **B. Gibson, D.G. WonyenandS. Chehreh Chelgani**: A review of pretreatment of diasporic bauxite ores by flotation separation. *Miner. Eng.*, **114**, 64-73 (2017)

2. **Weiwei Huang, Shaobin WangandZhonghua Zhu**: Phosphate removal from wastewater using RM. *J. Hazard. Mater.*, **158**, 35-42 (2008)

3. **Ahmed M. Yousif, Michael RodgersandEoghan Clifford**: Studying the Adsorption Properties of Modified RM towards Phosphate Removal from its Solutions. *International Journal of Environmental Science and Development*, **4**, 354-356 (2012)

4. **S.J. ShiaoandK. Akashi**: Phosphate Removal from Aqueous Solution from Activated RM. *Journal (Water Pollution Control Federation)*, **49**, 280-285 (1977)

5. **G. Akay, B. KeskinlerandA. çakici**: Phosphate removal from water by RM using crossflow microfiltration. *Water Res.*, **32**, 717-726 (1998)

6. **Hanrui Wang, Qiongchun Li and Shaohua Ju:** Preparration and Characterization of New Porous Granular RM Adsorbent Materail. *Nonferrous Metals (Mining Section)*, **8**,70-73 (2016)

7. Yaqin Zhao: Preparation and Characterization of a Novel RM Granular
Adsorbent for Phosphate Removal, Shandong University (2013)

8. **Y. Yin, G. XuandY. Xu**: Adsorption of inorganic and organic phosphorus onto polypyrrole modified RM: Evidence from batch and column experiments. *Chemosphere*, **286**, 131862 (2022)

9. **X. Li, M. JiandL.D. Nghiem**: A novel RM adsorbent for phosphorus and diclofenac removal from wastewater. *J. Mol. Liq.*, **303**, 112286 (2020)

10. **C.T.M. Witte, S. BlankenburgandE. Rauls**: Methane adsorption on graphene from first principles including dispersion interaction. *Surf. Sci.*, **605**, 746-749 (2011)

11. **Nian Xiang Qiu, Ying XueandYong Guo**: Adsorption of methane on carbon models of coal surface studied by the density functional theory including dispersion correction (DFT-D3). *Comput. Theor. Chem.*, **992**, 37-47 (2012)

12. **B. Zhang, W. LiangandP. Ranjith**: Effects of Coal Deformation on Different-Phase CO_2 Permeability in Sub-Bituminous Coal: An Experimental Investigation. *Energies*, **11**, 2926 (2018)

13. **Xin Gao, Qu ZhouandJingxuan Wang**: Adsorption of SO2 molecule on Ni-doped and Pd-doped graphene based on first-principle study. *Appl. Surf. Sci.*, **517**, 146180 (2020)

14. **W.D. Hsu, M. IchihashiandT. Kondow**: Ab initio molecular dynamics study of methanol adsorption on copper clusters. *J. Phys. Chem. A*, **111**, 441-449 (2007)

15. **Carlos F. Sanz-Navarro, Per-Olof ÅstrandandDe Chen**:
Molecular Dynamics Simulations of Carbon-Supported Ni Clusters Using the Reax Reactive Force Field. *The Journal of Physical Chemistry C*, **33**, 12663-12668 (2008)

16. **Masashi Nakamura, Yuma TanakaandMasamitu Takahasi**: Structural Dynamics of Adsorption Equilibrium for Iodine Adsorbed on Au(111). *The Journal of Physical Chemistry C*, **124**, 17711-17716 (2020)

17. **Biao Hu, Yuanping ChengandXinxin He**: Effects of equilibrium time and adsorption models on the characterization of coal pore structures based on statistical analysis of adsorption equilibrium and disequilibrium data. *Fuel*, **28**, 118770 (2020)

18. **A. M. Tolmachev, K. M. AnuchinandP. E. Fomenkov**: A Molecular Dynamics Study of the

Adsorption Equilibrium and Density Of Adsorbates. *J. Struct. Chem.+*, **59**, 1952-1959 (2018)
19. **Hongguang SuiandJun Yao**: Effect of surface chemistry for CH_4/CO_2 adsorption in kerogen: A molecular simulation study. *J. Nat. Gas Sci. Eng.*, **31**, 738-746 (2016)
20. **D. Gurina, O. SurovandM. Voronova**: Molecular Dynamics Simulation of Polyacrylamide Adsorption on Cellulose Nanocrystals. *Nanomaterials (Basel)*, **10** (2020)
21. **Z. Chen, W. MaandG. Lu**: Parallel-slipped pi-pi electron-donor-acceptor in adsorption process: Molecular dynamics simulation. *J. Mol. Graph. Model.*, **111**, 108100 (2021)
22. **Bin Zhang, Jianting KangandTianhe Kang**: Effect of water on methane adsorption on the kaolinite (001) surface based on molecular simulations. *Appl. Surf. Sci.*, **439**, 792-800 (2018)
23. **K. Wang, B. ZhangandT. Kang**: Effect of Geological Depths on CH4 Adsorption, Diffusion, and Swelling in Kaolinite by Molecular Simulations. *Energ. Fuel.*, **34**, 1620-1626 (2020)
24. **Chao Zhang, Jianbo WangandRenpeng Chen**: Water adsorption isotherms on soil external particle surface by molecular simulation. *Comput. Geotech.*, **139**, 104432 (2021)
25. **K. Kim, J.W. HanandK.S. Lee**: Promoting alkali and alkaline-earth metals on MgO for enhancing CO_2 capture by first-principles calculations. *Phys. Chem. Chem. Phys.*, **16**, 24818-24823 (2014)
26. **D.E. JiangandE.A. Carter**: Adsorption and dissociation of CO on Fe(110) from first principles. *Surf. Sci.*, **570**, 167-177 (2004)
27. **Jin-You Lu, Chia-Yun LaiandIbraheem Almansoori**: The evolution in graphitic surface wettability with first-principles quantum simulations: the counterintuitive role of water. *Phys. Chem. Chem. Phys.*, 22636-22644 (2018)
28. **Zongshang Guo**, *Journal of Institute of Mineral Deposits, Chinese Academy of Geological Sciences Number One.* (Geological Publishing House, Beijing, 1990)
29. Joseph I. Goldstein, Dale E. NewburyandJoseph R. Michael, *Scanningelectron microscopy and X -ray microanalysis*. (Berlin:Springer, 2018)
30. **J.J. Scott**: Analytical advances in the SEM. *Anal. Bioanal. Chem.*, **375**, 38-40 (2003)